Review Article

X-Ray Diffraction Investigations of Solutions

Georg Johansson

Department of Inorganic Chemistry, Royal Institute of Technology, S-100 44 Stockholm, Sweden

Johansson, G., 1989. X-Ray Diffraction Investigations of Solutions. – Acta Chem. Scand. 43: 307–321.

Methods for deriving structures of complexes in solution from X-ray diffraction data are reviewed. Some examples of structure determinations are discussed in order to illustrate how the method can be used and its limitations.

X-Ray diffraction measurements on solutions can lead to structural information on dissolved complexes which cannot be directly obtained by other methods. Although the diffraction effects are weak they can be efficiently analyzed as a result of improved measuring and data handling techniques, and an increasing number of solution diffraction investigations are being carried out. Ordinary laboratory X-ray equipment can be used for the data collection, and computer programs for handling and analysis of the data are available.[1] The information contained in the one-dimensional diffraction curve is limited and may not allow a unique interpretation in terms of complete three-dimensional structures for the complexes; however, significant structural information can usually be derived. In the following a survey of the method is given and some examples of structure determinations are discussed to show limitations and potentials of the method.

Experimental data

An experimental arrangement for measuring X-ray scattering from a solution is illustrated in Fig. 1. X-rays, usually Mo$K\alpha$ radiation with a wavelength λ = 0.7107 Å, are scattered from the free surface of the solution in a θ-θ diffractometer using the Bragg-Brentano parafocusing geometry. The scattered intensity is reflected in a focusing single-crystal monochromator of lithium fluoride before reaching the scintillation counter. The intensity is measured as a function of θ, the total scattering angle being 2θ, and different slit widths are used to cover the total θ range. In the high-angle region, which is of primary importance for investigating structures of complexes, the diffraction effects correspond to variations in the intensity of less than a few per cent, and in order to obtain sufficient statistical accuracy in the counting, long measuring times at discrete intervals of θ are needed. After corrections for background radiation and for absorption in the sample, data from different θ ranges are scaled to a common slit width. The final data set produced by the computer consists of the observed intensity values as a function of $s = 4\pi\lambda^{-1}\sin\theta$. For Mo$K\alpha$ radiation, $s_{max} \approx 16$ Å^{-1}. For Ag$K\alpha$ radiation, with λ = 0.5608 Å, $s_{max} \approx 21$ Å^{-1}.

Theoretical background

The ordered arrangement in a crystal leads to a distinct three-dimensional diffraction pattern from which a unique structure can almost always be derived, and precise values for the limited number of parameters needed to describe the structure can be determined. A non-ordered substance,

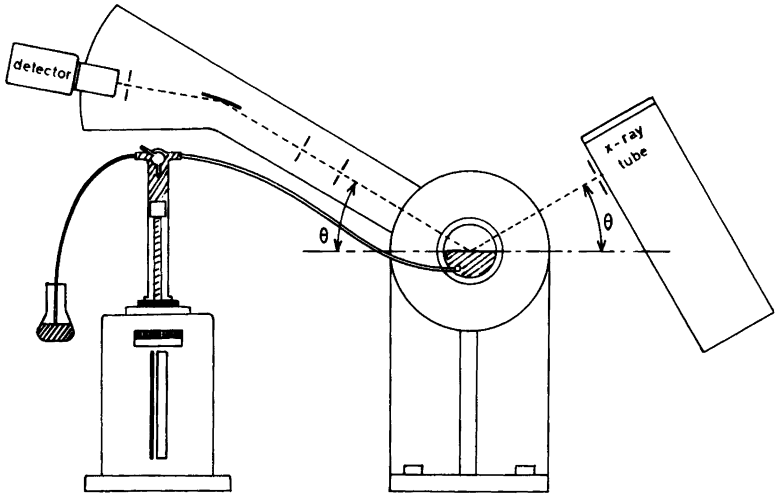

Fig. 1. Experimental arrangement for X-ray diffraction measurements on solutions with the use of a θ–θ diffractometer.

if it is a liquid, a solution or an amorphous solid, gives a one-dimensional, weak and rather diffuse diffraction pattern, and the description of its structure is not as simple as that of a crystal.

The structure can be described by correlation functions, $g_{pq}(r)$, which give the time averaged probability of finding a particle "q" at a distance r from a particle "p". If the particles are atoms, the number of "q" atoms in a spherical shell of radius r surrounding a "p" atom is then given by the expression:

$$dn = n_q V^{-1} 4\pi r^2 g_{pq}(r)\, dr$$

where n_q is the number of atoms "q" in a unit volume V. The Fourier transform of the correlation function gives the partial structure factor $S_{pq}(s)$:

$$S_{pq}(s) = 1 + 4\pi N V^{-1} s^{-1} \int [g_{pq}(r) - 1] \cdot r \cdot \sin(rs) \cdot dr$$

Here, N is the number of particles in the volume V and $s = 4\pi\lambda^{-1} \sin\theta$.

When the partial structure factor is known the corresponding correlation function can be calculated by a Fourier transformation:

$$g_{pq}(r) = 1 + V(2\pi^2 Nr)^{-1} \int (S_{pq}(s) - 1) \cdot s \cdot \sin(rs) \cdot ds$$

For a solution containing n different atomic species, the total structure factor is obtained as a sum over the $n(n+1)/2$ different partial structure factors and the total correlation function is the sum over the corresponding partial correlation functions. The total scattered intensity measured as a function of s in an X-ray diffraction experiment and normalized to a unit volume is equal to

$$I(s) = \Sigma n_p f_p^2(s) + \Sigma\Sigma n_p n_q f_p(s) f_q(s) [S_{pq}(s) - 1]$$

where $f(s)$ are the X-ray scattering factors for the atoms. For large values of s the structure factors, $S(s)$, approach unity, which can be used for normalization of the observed intensities to a unit of volume chosen. By subtracting the independent coherent scattering term, $\Sigma n_p f_p^2(s)$, from the normalized intensity values the reduced intensity function $i(s)$, which contains the structural information on the solution, is obtained:

$$i(s) = I(s) - \Sigma n_p f_p^2(s) = \Sigma\Sigma n_p n_q f_p(s) f_q(s) [S_{pq}(s) - 1]$$

Since the X-ray scattering factors, $f(s)$, are functions of s the measured intensities are not linear combinations of the different partial structure factors, and a Fourier transformation results in a convoluted correlation function. For X-rays, the scattering factors are roughly proportional to the number of electrons in an atom. Since the contribution to $i(s)$ is weighted by the product of the scattering factors, light atoms will contribute less than heavy atoms and will be more difficult to locate.

An electronic radial distribution function, $D(r)$, can be calculated from the observed $i(s)$ values, and is defined by the expression:

$$D(r) = 4\pi r^2 \varrho_o + 2r\pi^{-1} \int s \cdot i(s) \cdot M(s) \cdot \sin(rs) \cdot ds$$

where $\varrho_o = (\Sigma n_p Z_p)^2 / V$ and $\Sigma(n_p Z_p)$ is the total number of electrons in the unit volume. $M(s)$ is a sharpening function introduced to compensate for the decrease in the scattering factors with increasing s.

Interpretation of the diffraction data

Diffraction data for a solution can be analyzed either in s space, from the intensity data, or in r space, from the radial distribution functions. The procedure will be illustrated for an aqueous erbium chloride solution, which has been chosen because it offers the possibility of separating interactions by using isomorphic substitution. This allows more detailed structural information to be derived than is usually possible.

The observed intensities are corrected for multiple scattering, polarization and incoherently scattered radiation, which is only partially removed by the monochromator. After normalization to a unit volume containing one Er^{3+} ion, carried out by comparing observed values in the high-angle part of the intensity curve with the total independent coherent scattering, $\Sigma n_p f_p^2(s)$, the reduced intensities, $i(s)$, are calculated from the normalized $I(s)$ values by subtracting $\Sigma n_p f_p^2(s)$.[1] For a 2.4 M $ErCl_3$ solution, Fig. 2 shows the $I(s)$ values, the total independent coherent scattering, the estimated amount of incoherent scattering reaching the detector and the reduced intensity values, $i(s)$, which contain the structural information.

The radial distribution function, $D(r)$, calculated with the use of a sharpening function $M(s) = f_o(0)^2 f_o(s)^{-2} \exp(-0.01s^2)$, and the reduced RDF, $D(r) - 4\pi r^2 \varrho_o$, which gives the variation of $D(r)$ around the average $4\pi r^2 \varrho_o$, are shown in Fig. 3. Since the experimental intensity data have an upper cut-off limit, in this case $s_{max} \approx 20$ Å^{-1} since Ag$K\alpha$ radiation was used, the sharpening function has to be chosen such as to give an optimal sharpening without introducing large cut-off errors in the RDF.

Intramolecular interactions. A peak at 2.34 Å in the radial distribution function indicates Er-H_2O bonding distances (Fig. 3). A similar distance is found for hydrated erbium ions in crystal structures. The parameter values characterizing the Er-H_2O interactions can be estimated by comparison with theoretical peaks. For sharp interactions between two atoms "p" and "q", resulting from well-defined intramolecular distances, r_{pq}, the contribution to the intensity curve can be calculated from the Debye expression:

$$i(s) = 2\Sigma\Sigma f_p(s) f_q(s) (r_{pq} s)^{-1} \sin(r_{pq} s) \times \exp(-\tfrac{1}{2} l_{pq}^2 s^2)$$

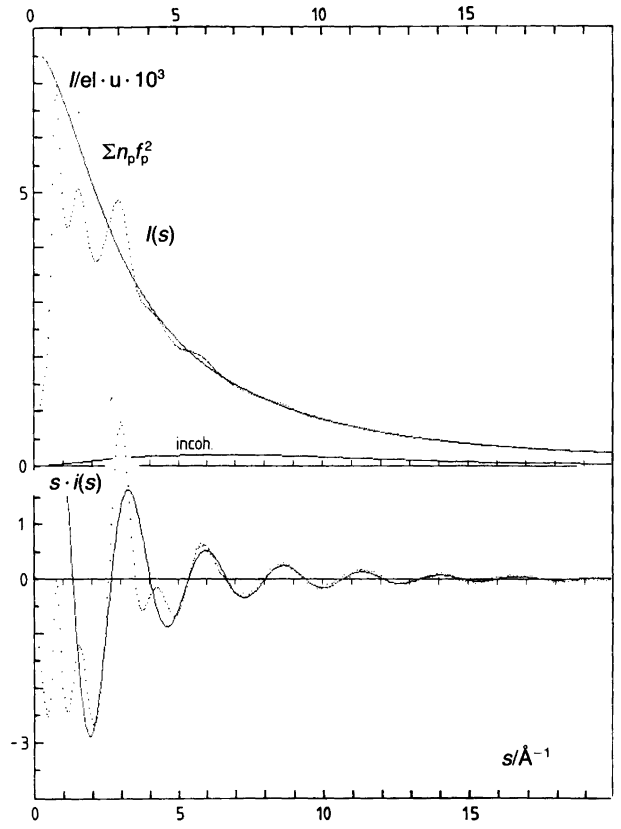

Fig. 2. Results of diffraction measurements on a 2.4 M erbium chloride solution. Observed intensity values, $I(s)$, the total independent coherent scattering, $\Sigma n_p f_p(s)^2$, and the fraction of incoherent scattering reaching the detector are shown in the upper part. In the lower part of the figure the reduced intensity values, $s \cdot i(s)$, are compared with theoretical values calculated by including only Er-H_2O interactions from the 1st coordination sphere (r = 2.34 Å, n = 8.0, l = 0.10 Å).

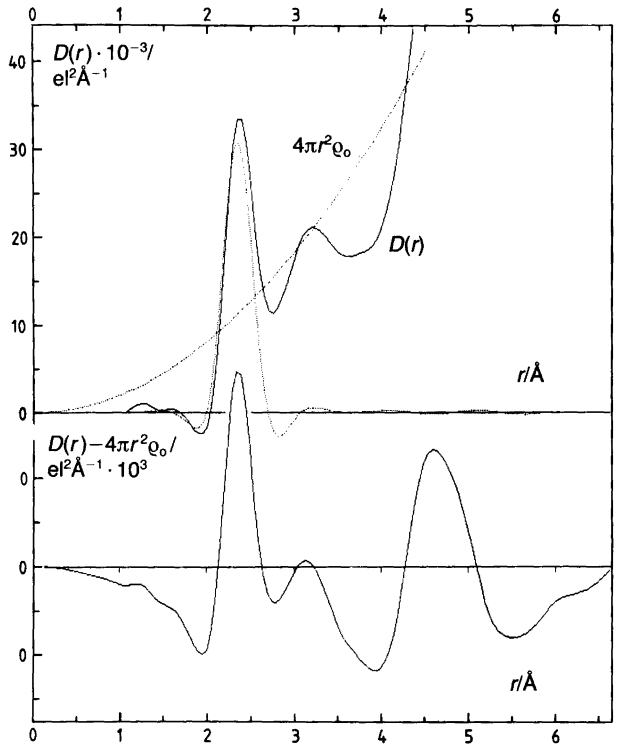

Fig. 3. RDF's for a 2.4 M $ErCl_3$ solution. The upper part shows the radial distribution function, $D(r)$, the average function, $4\pi r^2\varrho_0$, and a theoretical peak calculated for Er-H_2O interactions of the 1st coordination sphere (r = 2.34 Å, n = 8.0, l = 0.10 Å). The lower part gives the reduced radial distribution function $D(r)-4\pi r^2\varrho_0$. Data are normalized to a unit volume containing one Er atom.

This assumes a Gaussian distribution of each distance around its average, with a root-mean-square variation of l_{pq} Å. It follows from this expression that sharp interactions with low l_{pq} values will give more distinct contributions to the high-angle part of the intensity curve than those interactions which have larger rms variations or have no well-defined distances to surrounding atoms. This can be used to separate intra- and intermolecular interactions in the $i(s)$ curves.

The contribution of a sharp interaction to the $D(r)$ function can be obtained by a Fourier transformation of the theoretical $i(s)$ values analogous to that used for the experimental $i(s)$ values. An interaction with a small rms variation will lead to a sharp peak in the RDF, which can usually be distinguished from the diffuse peaks resulting from distances between non-bonded atoms.

In Fig. 3, the Er-H_2O peak at 2.34 Å is partly overlapped by the neighboring peak at about 3.1 Å, which is composed of H_2O-H_2O interactions, expected at about 2.9 Å, and $Cl-H_2O$ interactions, expected at about 3.2 Å. Without knowing the contributions from these interactions a derivation of the parameters characterizing the hydration sphere around Er^{3+}, by comparison with theoretical peaks, will be uncertain. As illustrated in Fig. 4 for a 1 M $ErCl_3$ solution, this will become more pronounced for more dilute solutions, where the metal-water interactions become less dominant. From the size of the peaks an approximate coordination number of about eight can be derived for the 1st coordination sphere of the erbium ion.

The contributions from these Er-H_2O distances to the reduced intensities for the 2.4 M solution, as calculated from the Debye expression, are compared in Fig. 2 with the observed $i(s)$ values. They are the dominant contributions in the high-angle part of the curve and can, therefore, be analyzed in terms of a distance, r, a frequency, n, and a rms variation, l, by a direct comparison of observed and theoretical $i(s)$ values using a least-squares procedure, excluding the low-angle part of the intensity curve, where other interactions in the solution make large contributions. This requires, however, that the remaining structure in the solution does not give significant contributions to the intensity curve in the s region used. The strong correlation between the frequency of a distance, n_{pq}, and its rms variation, l_{pq}, also requires a sufficiently extended region of the intensity curve in which the interaction is dominant, and this is not often available.

A possible 2nd coordination sphere around Er^{3+} is in-

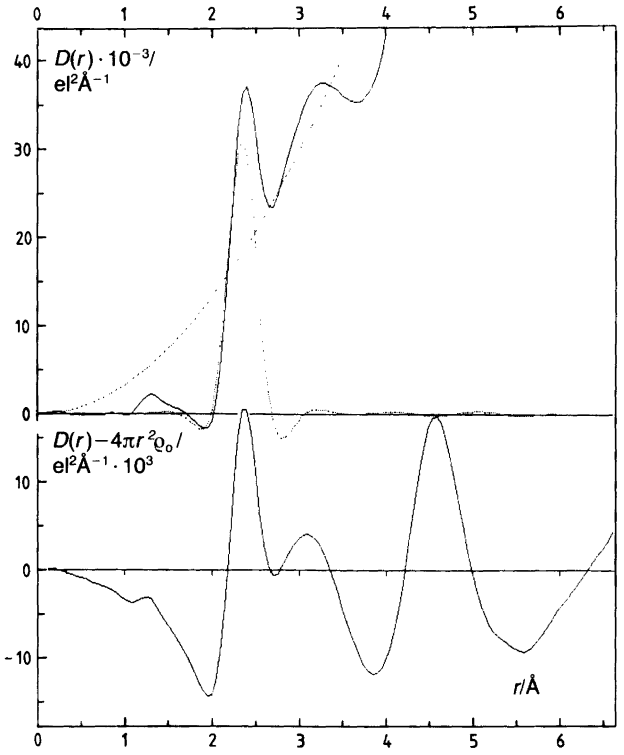

Fig. 4. RDF's for a 1.0 M $ErCl_3$ solution. The $D(r)$ function (solid line), the $4\pi r^2\varrho_0$ function (dotted line) and a theoretical Er-H_2O peak calculated for r = 2.34 Å, n = 8.0 and l = 0.10 Å are shown in the upper part. Data are normalized to a unit volume containing one Er atom.

dicated at about 4.6 Å in the RDF's, but occurs in a region where a large number of other interactions will also contribute (Figs. 3 and 4), thus preventing a quantitative analysis of the shape and the size of this peak.

Isomorphic substitution. For a precise analysis of the 1st and 2nd coordination spheres a separation of the corresponding peaks from overlapping peaks is necessary and can, in this particular case, be achieved by means of isomorphic substitution.[2] The $ErCl_3$ solution contains four different atomic species: the metal ion "M", the ligand "L", oxygen "O" and hydrogen "H", and the total number of partial distribution functions is ten, each of which contributes to the $i(s)$ function. If a substituent ion M′ can be found, which has a scattering power differing from that of M, but which does not change the structure of the solution when replacing M, the $i(s)$ function for the "M′" solution will be the same as for the "M" solution, except for terms involving the metal ions. If the number of atoms of each type in the unit volume is given by n_M, n_L, n_O and n_H, respectively, we can write the following equation for the difference, $\Delta i(s)$, between observed intensities for two solutions of the same compositions, one containing M and the other M′:

$$\Delta i(s) = 2n_M n_O f_O\, \Delta f_M[S_{MO}(s)-1] + 2n_M n_L f_L\, \Delta f_M[S_{ML}-1] + 2n_M n_H f_H\, \Delta f_M[S_{MH}(s)-1] + n_M^2(f_M^2-f_{M'}^2)[S_{MM}(s)-1]$$

where $\Delta f_M = f_M - f_{M'}$ and terms not involving the metal ions are eliminated. Normally, the first two terms will be much larger than those involving MH and MM interactions. A deconvolution of these terms in the difference function is obtained by the Fourier transformation:

$$D^M(r) = 4\pi r^2\varrho_o^M + 2r\pi^{-1}\int s\cdot\Delta i(s)\cdot\sin(rs)\cdot M(s)\cdot f_M(\Delta f_M)^{-1}\cdot ds$$

where $\varrho_o^M = (\Sigma n_1 Z_1)^2/V$ includes only terms involving the metal ion.

The trivalent erbium ion has the outer electron configuration $4s^2p^6d^{10}f^{11}5s^2p^6$ and is chemically closely related to the trivalent yttrium ion with the configuration $3s^2p^6d^{10}4s^2p^6$. As a result of the lanthanide contraction, the ionic radius for the Y^{3+} ion is about the same as that found for the elements close to Er^{3+} in the lanthanide series. A solution of an erbium salt can, therefore, be expected not to change its structure if Er^{3+} is replaced by Y^{3+}. This is confirmed by diffraction measurements, and can be used to separate interactions involving the erbium ion from other interactions by using the difference between the scattering curves for two solutions of the same composition, one containing Er^{3+} and the other Y^{3+}.

The results for the $ErCl_3$ solutions are shown in Figs. 5 and 6. In the separated RDF's, the 2.4 Å peak and the 4.6 Å peak from the RDF's in Figs. 3 and 4 now appear among the Er interactions, and the 3.1 Å peak among the non-Er interactions (Figs. 5 and 6). The 2.4 Å peak is fully separated in both solutions, and is closely reproduced by a calculated Gaussian peak corresponding to 8.0 Er-H_2O interactions at 2.34 Å with an rms variation l_{pq} = 0.10 Å. The same parameter values are found to be valid for both the 1 M and the 2.4 M solution (Figs. 5 and 6). The 1st coordination sphere thus does not seem to be significantly affected by the difference in concentration and there are no indications of Cl^- ions bonded within the 1st coordination sphere. The peak, therefore, represents only metal-water bonding distances within the hydrated metal ion.

The presence of the 4.6 Å peak among the Er interactions in Figs. 5 and 6 proves that it results from a 2nd coordination sphere around the Er^{3+} ion. Although apparently not a Gaussian peak, it can be approximately reproduced for the 1M solution by a theoretical Er-H_2O peak calculated for r = 4.62 Å, n = 15.0 and l = 0.28 Å. In the concentrated solution its shape has broadened and it appears as a double peak, presumably because Cl^- ions are now incorporated into the 2nd coordination sphere, forming outer-sphere complexes.

The peak at about 3.1 Å (Figs. 3 and 4) appears among the non-erbium interactions (Figs. 5 and 6), which proves that it results from water–water interactions involving bonded as well as non-bonded water molecules and expected at about 2.9 Å, and chloride-water interactions, which are expected at about 3.2 Å. The different interactions are not resolved and the peaks cannot be reproduced by Gaussian peaks.

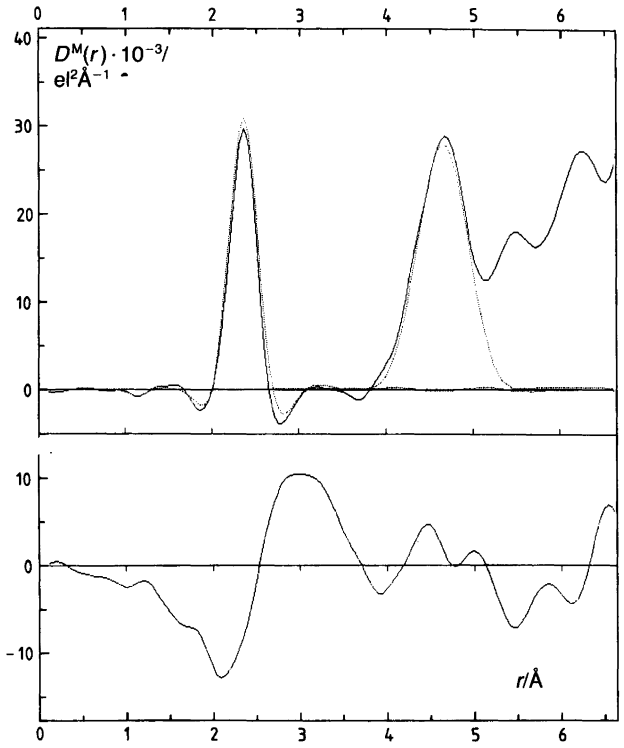

Fig. 5. Separated RDF's for a 1.0 M $ErCl_3$ solution. The upper part shows the $D^M(r)$ function (solid line), which includes only interactions involving erbium. Two theoretical Er-H_2O peaks (dotted lines) are calculated for r = 2.34 Å, n = 8.0, l = 0.10 Å and for r = 4.62 Å, n = 15.0, l = 0.28 Å. The lower part shows the reduced RDF after subtracting contributions from interactions involving erbium. Data are normalized to one Er atom.

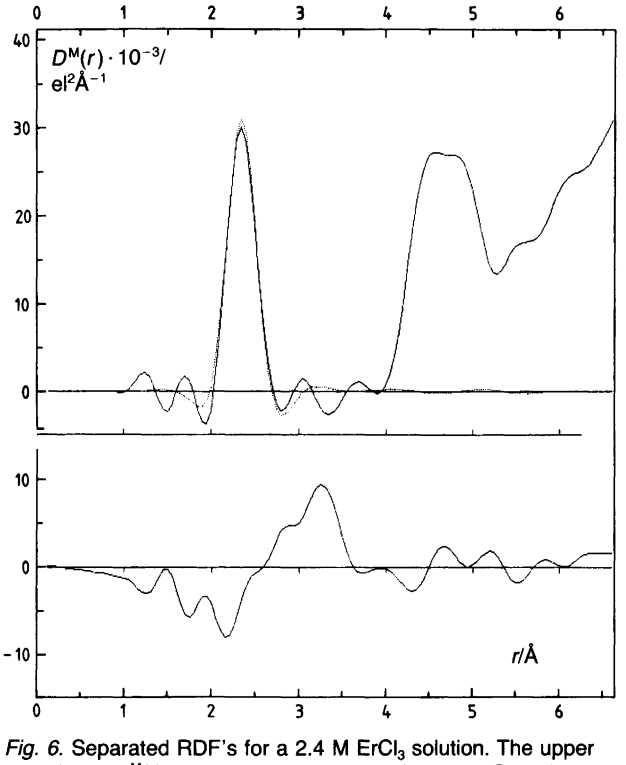

Fig. 6. Separated RDF's for a 2.4 M $ErCl_3$ solution. The upper part shows $D^M(r)$ (solid line) and a theoretical Er-H_2O peak calculated for r = 2.34 Å, n = 8.0 and l = 0.10 Å. The lower part gives the reduced RDF after eliminating interactions involving erbium. Data are referred to one Er atom.

The number of available "isomorphic" pairs of atoms is limited and this method of separation of interactions cannot often be used. The results derived for the $ErCl_3$ solutions can, however, be taken as representative for other solutions. Strong interactions, corresponding to well-defined intramolecular distances, can be closely reproduced by theoretical peaks, assuming a Gaussian distribution of the distances. These specific characteristics of the intramolecular interactions make their separation from other types of interactions in solution possible, and they can be analyzed, at least approximately, in terms of distance and frequency even if a separation of interactions cannot be made. Other types of interactions cannot be described by Gaussian peaks and they are not usually resolved into single peaks. Although it will probably be possible to resolve an RDF into a number of Gaussian peaks, this may not necessarily have any physical significance.

For a complex chemical system, the significant information that can be extracted from a single diffraction curve is therefore limited to the parameters characterizing the sharp interactions resulting from intramolecular distances. The remaining structure in the solution cannot usually be determined. Interactions involving strongly scattering atoms will be more dominant and more favorable for an analysis than light atoms. By using a suitable sharpening function for the Fourier transformation the resolution of a peak in the RDF from the background can be optimized. Cut-off errors caused by the non-infinite value for the upper integration limit will not seriously affect this analysis, since corresponding effects will appear in the theoretical curve.

The sharp interactions will also be the dominant contributors to the high-angle part of an intensity curve, and may also be analyzed by a direct comparison of observed and calculated intensity values in that region of the curve. The strong correlation between the frequency of a distance and its rms variation may, however, easily lead to systematic errors in the parameter values.

Hydration numbers

A large number of diffraction measurements have been carried out for electrolyte solutions, primarily in order to determine the structures of hydrated metal ions. In a limited number of systems this can be done by separating the partial distribution functions. In neutron diffraction, when combined with isotopic substitutions, difference methods have been used for this purpose. This latter technique is the equivalent of isomorphic substitution in X-ray diffraction, but has the advantage of being less likely to effect the structure of the solution.[3,4] Ions investigated include Li^+, K^+, Ca^{2+}, Cu^{2+}, Ni^{2+}, Nd^{3+}, Dy^{3+}, Ag^+ and Cl^-.[5] For most

systems, however, this technique cannot be used and an analysis has to be based on a single diffraction curve for a concentrated solution of the metal salt.

An often used method for analyzing the data is the so-called "first neighbor model"[6] in which discrete interactions, each described by a distance, r_{pq}, its frequency, n_{pq}, and its rms variation, l_{pq}, are introduced for cation–water and anion–water contacts in the solution, while other interactions are approximated by an evenly distributed electron density surrounding each atom outside a sphere of radius R. The water structure is assumed to be the same as in pure water and is included in the model by taking into account the mole fraction of water in the solution. The coordination polyhedra are assumed to have the same high symmetry that is found in crystal structures, usually octahedral or tetrahedral, and the coordination numbers are assumed to be integers. The parameters of the model are then refined by a least-squares procedure comparing calculated intensities for the model with experimental values.

In a development of this approach some of the constraints in the original model have been lifted, leading to better final agreement between observed and calculated data, but also to a larger number of parameters to be refined.[7] The water structure is included in the refinement by introducing water–water interactions. A 2nd coordination sphere is introduced for the cations and the symmetry requirements for the coordination polyhedra are dropped, allowing non-integral values for the coordination numbers. The final agreement between observed and calculated $i(s)$ values is usually excellent over the whole s range and coordination numbers derived are reasonable, when compared to values found in crystals. It is difficult, however, to assess the accuracy of the derived parameter values considering the large number of parameters in relation to the limited one-dimensional data set, the strong correlation between the frequency of an interaction and its rms variation, the assumption of a gaussian distribution of distances even for the water–water interactions and for the assumed 2nd coordination sphere, and the obvious approximations inherent in the assumptions about the emergence of the continuum around the atoms. The possibility of complex formation in the system will further complicate attempts to construct a realistic, non-biased model for the solution.

Lists of hydration numbers derived from diffraction measurements have been given in several review articles.[4,7–9]

Complex formation

Most investigations of structures of complexes in solution have involved halide complexes of metal ions. For chloro complexes, the metal-chloride bonding distances usually fall between metal–water bonding distances and water–water contact distances. They will often appear in an RDF as a partially resolved peak, which can be analyzed in terms of distance and frequency. For bromo and iodo complexes, the heavier ligand atoms will give stronger contributions to the scattering curves. The metal halide and halide-halide peaks will stand out above the background and can be analyzed, although they appear at longer distances where they are overlapped by contributions from other types of interactions. Results of structure determinations reported in the literature are listed in Table 1.

Gold(III) is an example of a metal ion forming only one dominant halide complex, AuX_4^-, the structure of which can be uniquely and accurately determined from solution diffraction data alone.[10] Diffraction curves for 3 M $HAuBr_4$ and $HAuCl_4$ solutions are shown in Fig. 7, and the corresponding radial distribution curves in Fig. 9. The intramolecular interactions can be easily identified by the peaks at 2.42 Å, 3.4 Å, and 4.9 Å for the bromide solution and 2.29 Å, 3.2 Å, and 4.6 Å for the chloride solution. The 2.42 Å and the 2.29 Å peaks correspond to values found in crystal structures for Au-Br and Au-Cl bonding distances, respectively. The size of these peaks, as estimated from a comparison with calculated peaks, correspond to 4 X^- bonded to each Au^{3+}. The ratios between the distances are for each solution $1 : \sqrt{2} : 2$, which is consistent only with a square-planar AuX_4^- complex. A least-squares refinement comparing observed intensities with calculated values, including only the intramolecular interactions of the AuX_4^- complexes, leads to the parameter values given in Table 1. The agreement between observed and calculated values (Fig. 7) shows the intramolecular interactions to be totally

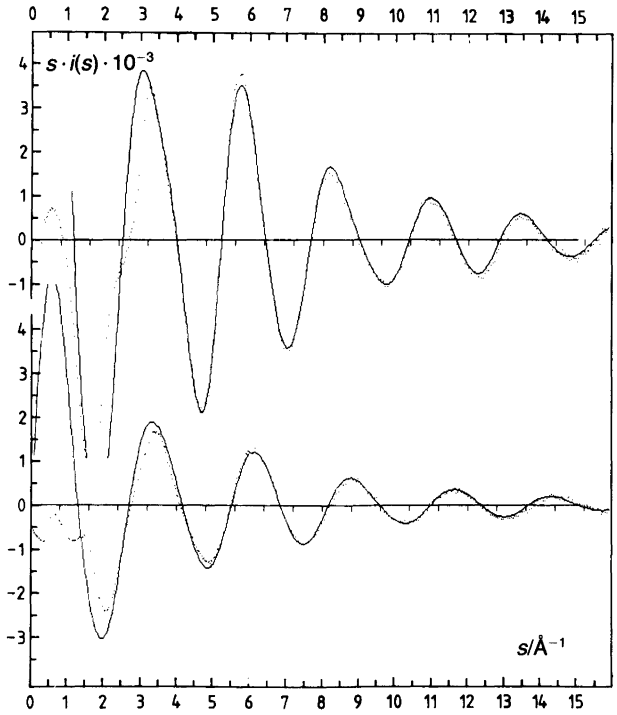

Fig. 7. Experimental $s \cdot i(s)$ values (dots) for 3 M solutions of $HAuBr_4$ (upper curve) and $HAuCl_4$ (lower curve) compared with theoretical values (solid lines) calculated by including only intramolecular interactions.

Table 1. Structure of halide complexes derived from solution diffraction data. The metal ion, M, the ligand, L, and the solvent used, are given. The derived composition of the complex and its suggested symmetry, or the average number, *n*, of ligands bonded to each metal ion, are included. The metal-ligand distance, *d*, and the rms variation, *l*, are also listed.

M	L	Solv.	[M]/mol l^{-1}	[L]/[M]	Complex		*d*/Å	*l*/Å	Ref.
Ag(I)	I^-	Aq[a]	<3.7	2.9–6.3	AgI_4^{3-}		2.9		37
	I^-	Melt		0.07–0.61	AgI_4^{3-} p.n.		2.82	0.17	23
	I^-	Aq	9.0–11.0	0.09–0.11	Ag_4I^{3+}		2.82(1)	0.14	22
	I^-	Tht[a]	1.77	1.0	$(AgISC_4H_8)_4$		2.824(4)	0.36(10)	39
	I^-	DMSO	0.5–1.0	1.5–4.0	AgI_3^{2-}p.n.		2.78–2.86	0.14	38
	Br^-	Tht	1.45	1.0	$(AgBrSC_4H_8)_4$		2.592(3)	0.06(3)	39
Au(III)	Br^-	Aq	2.77	4.6	$AuBr_4^-$ sq.pl.		2.432(3)	0.05(4)	10
	Cl^-	Aq	3.13	4.4	$AuCl_4^-$ sq.pl.		2.291(2)	0.07(4)	10
Cd(II)	I^-	Aq	2.25	5.1	CdI_4^{2-}	T	2.79	0.089	40
	I^-	Aq	1.27	0.72	$CdI(H_2O)_5^+$	O	2.80(5)	0.081	41
	I^-	DMSO[a]	1.33	3.8	CdI_4^{2-}	T	2.790(3)	0.08(4)	42
			1.70	3.0	CdI_3^-	P	2.773(3)	0.08(4)	42
	Cl^-	Aq	0.9–1.3	2.0	$n = 2$		2.569(4)	0.15(3)	43
	Cl^-	Aq	1.3 m	2.0	$n = 1.75(8)$		2.576(2)	0.080(6)	83
Co(II)	Br^-	Aq	2.8–4.3	2.0	$n = 0.3–0.6$		2.58	0.12	44
	Cl^-	Aq	2.97	2.0	$CoCl(H_2O)_5^+$		2.47(1)	0.10	45
	Cl^-	Aq	0.6	22	$CoCl_4^{2-}$	T	2.29		46
			2.13	3.4	$CoCl(H_2O)_5^+$		2.35		46
	Cl^-	Aq	2.1 m	4.2	$n = 0.96(9)$		2.437(5)	0.14(1)	47
	Cl^-	Aq	0.98	6.1–7.2	$n = 0.22–1.13$		2.36–2.37	0.18–0.14	48
Cr(III)	Cl^-	Aq	1.9–2.8	3.0–4.9	$n = 0.65–1.5$		2.31(2)	0.09	49
Cu(II)	Br^-	Aq	1.0–4.4	2.0–6.7	$n = 0.33–3.85$		2.42–2.46		50
	Cl^-	Aq	3.7	2.5	$n = 4.0$		2.27, 2.6		51
	Cl^-	Aq	2.95	2.0	$n = 1.2$		2.250(2)	0.10(2)	45
Fe(II)	Br^-	Aq	2.7–4.5	2.0	$n = 0.33–0.75$		2.61–2.62	0.12	44
Fe(III)	Cl^-	Aq	1.5–5.0	3.0	$FeCl_6^{3-}$, Fe_2Cl_6		2.3		52
	Cl^-	Aq	5.0		$FeCl_4(H_2O)_2$		2.3		53
	Cl^-	Aq	2.2–5.9	3.0–4.7	$FeCl_n(H_2O)_{6-n}$ $FeCl_4^-$		2.24–2.37	0.05–0.3	54
	Cl^-	Aq	4.9–5.7	3.0	$n = 3.5–4.0$		2.28		55
	Cl^-	Aq	2.2	5.2	$FeCl_4^-$		2.26		56
	Cl^-	Aq	3.6–5.9	3.0–4.0	$n = 3.2–3.4$		2.21–2.36	0.05–0.1	57
	Cl^-	Meth[a]	6.0–11m	3.0	Fe_2Cl_6		2.25		58
Hg(II)	I^-	Aq		4	HgI_4^{2-}	T	2.78		59
	Cl^-	Aq		>4	$HgCl_4^{2-}$		2.51		59
	I^-	DMSO	0.9–2.5	2.0–4.0	HgI_4^{2-}	T	2.80	0.09(4)	12
		DMF[a]	1.0–2.0	3.0–4.0	HgI_3^-	P	2.73	0.11(4)	
					HgI_2	∠(165°)	2.60	0.07(4)	
	I^-	Aq	2.7–3.5	3.5–4.5	HgI_4^{2-}	T	2.785(3)	0.10(4)	60
					HgI_3^-	P	2.76	0.10(4)	
	Br^-	Aq	1.6–3.6	3.4–4.5	$HgBr_4^{2-}$	T	2.610(5)	0.11(7)	60
					$HgBr_3^-$	P	2.58	0.11(7)	
	Cl^-	Aq	1.0–5.0	2.8–5.8	$HgCl_4^{2-}$	T p.n.	2.47(1)	0.11(4)	60
	I^-	DMSO	1.3–4.4	1–2	HgI_2	∠(159°)	2.625(2)	0.07–0.09	14
	Br^-	DMSO	0.6–3.2	1–4	$HgBr_4^{2-}$	T	2.636(4)	0.07–0.11	14
					$HgBr_3^-$	P	2.548(4)		

contd

dominant over the whole angular range, except for the lowest *s* values. The individual contributions from the Au-X and the X-X interactions to the intensity curves are drawn separately in Fig. 8, and show a large dominance for the former, which is reflected in the accuracy with which the corresponding parameter values can be determined. The Cl-Cl contributions are too weak to allow a separate refinement of their parameters. Despite this the Cl-Cl peaks are clearly indicated in the RDF (Fig. 9).

After subtraction of the corresponding theoretical peaks from the RDF's only a diffuse background remains without any significant structural features (Fig. 9). In this particular case, with a single dominant complex containing strongly scattering atoms, the diffraction data are sufficient for a complete structure determination and lead to parameter values for the metal-ligand interactions of an accuracy comparable to that obtained in a crystal structure determination. The remaining structure in the solution is too weak to

Table 1. (contd)

M	L	Solv.	[M]/mol l^{-1}	[L]/[M]	Complex		*d*/Å	*l*/Å	Ref.
					$HgBr_2$	∠(165°)		2.455(3)	
	Cl^-	DMSO	1–1.5	1–3	$HgCl_3^-$ pl		2.434(4)	0–0.09	14
					$HgCl_2$		2.350(4)		
	Cl^-	Meth	1.5	2	$HgCl_2$		2.308(3)		14
	Br^-	DMSO	0.4	4.5	$HgBr_4^{2-}$	T	2.628(2)	0.12(2)	61
	Cl^-	DMSO	0.4	4.5	$HgCl_4^{2-}$		2.532(2)	0.05(3)	61
	I^-	Py[a]	0.7	2.0	$HgI_2(py)_2$		2.665(2)	0.070(6)	62
	Br^-	Py	0.7	2.0	$HgBr_2(py)_2$		2.497(2)	0.067(3)	62
	Cl^-	Py	0.9	2.0	$HgCl_2(py)_2$		2.375(10)	0.071(6)	62
	I^-	Py	1.20	1	CH_3HgI		2.649(3)	0.06	63
	Br^-	Py	1.43	1	CH_3HgBr		2.480(3)	0.08(3)	63
	Cl^-	Py	1.21	1	CH_3HgCl		2.325(8)	0.06	63
	I^-	Tht	0.72–0.83	2	$HgI_2(tht)_2$		2.670(4)	0.070(4)	64
	Br^-	Tht	0.72	2	$HgBr_2(tht)_2$		2.535(6)	0.086(6)	64
Gd(III)	Cl^-	Aq	1.55m	6.0	$GdCl_2(H_2O)_6^+$		2.8		65
La(III)	Cl^-	Meth	1.95m	3.0	$n = 3$		2.95		66
	Cl^-	Meth	2m	3.0	$n = 0$–4		2.95		67
Nd(III)	Cl^-	Aq, meth	1.5–1.9 m	6.0–3.0	$n = 1$–2		2.78		77
Mn^{2+}	Br^-	Aq	2.1–5.7	2.1–3.3	$n = 1.1$–1.2		2.60–2.64		84
	Cl^-	Aq	2.7–4.7	2.0–3.4	$n = 1.3$–1.5		2.49		84
Ni(II)	Br^-	Aq	2.0	2.0	$n = 0.15$		2.62(1)	0.09(1)	68
	Br^-	Aq	2.1–4.1	2.0	$n = 0.29$–0.44		2.61(1)	0.13(1)	69
	Br^-	Aq	2.0–4.8	2.0	$n = 0.18$–0.68		2.52–2.58	0.12	70
	Cl^-	Aq	2.95	2.0	$Ni(H_2O)_5Cl^+$		2.44(1)	0.10	45
	Cl^-	Aq	1.98	4.0–5.0	$n = 0.92$–1.43		2.44–2.47	0.14	71
Pt(IV)	Br^-	Aq	2.74	6.25	$PtBr_6^{2-}$	O	2.47	0.077	11
	Cl^-	Aq	2.88	6.44	$PtCl_6^{2-}$	O	2.33	0.063	11
Rh(III)	Cl^-	Aq	0.39	4.86	$Rh(H_2O)_3Cl_3$		2.33(1)	0.05(1)	72
Tl(III)	I^-	CH_2Cl_2	0.77	4.0	TlI_4^-	T	2.771(3)	0.12(3)	73
	Br^-	Aq	1.0–2.7	2.0–12.3	$TlBr_2(H_2O)_4^+$		2.481(2)	0.06(3)	15
					$TlBr_3(H_2O)_2$		2.512(2)	0.06(3)	
					$TlBr_4^-$	T	2.564(1)	0.07(2)	
	Cl^-	Aq	0.92–2.65	4.1–13.4	$TlCl_4^-$	T	2.43(1)	0.10(3)	74
					$TlCl_6^{3-}$	O	2.59(1)	0.09(4)	
Zn(II)	Br^-	Aq	3.5–23m	2.0–4.3	$n = 2$–4		2.40		75
	Br^-	Acet[a]	4.2m	2.0	$n = 2$		2.40		75
	Br^-	Aq	1.64	3.1	$n = 2.26$		2.42	0.12	76
	Br^-	Aq	1.0–7.6	0–5.0	$ZnBr_4^{2-}$	T	2.406(4)	0.08	16
					$ZnBr_3^-$		2.386	0.08	
					$ZnBr_2$		2.386	0.08	
	Cl^-	Aq	5.0–27.5m	2.0	$ZnCl_n(H_2O_{4-n}$		2.28		78
	Cl^-	Aq	2.2–2.6	6.1–6.5	$ZnCl_4^{2-}$	T	2.30(1)		79
	Cl^-	Aq	2.2–2.3	2–6	$n = 2$–4		2.30		80
	Cl^-	Aq	2.68	2.0	$ZnCl(NH_3)_3^+$		2.30(3)		81
	Cl^-	Aq	2.2	2.0	$Zn(tren)Cl^+$		2.37(3)		82
	Cl^-	Aq	1.0 m	2.0	$n = 1.06(4)$		2.240(5)	0.111(5)	83

[a]Aq = water, Tht = tetrahydrothiophene, DMSO = dimethyl sulfoxide, Meth = methanol, DMF = dimethylformamide, Py = pyridine, Acet = acetone.

influence the results. Comparable results have been obtained for other similar complexes: $PtCl_6^{2-}$ and $PtBr_6^{2-}$,[11] HgI_4^{2-} and $HgBr_4^{2-}$,[12,14] $TlBr_4^-$,[15] $ZnBr_4^{2-}$ [16] (Table 1).

Metal ions usually form a series of complexes with a specific ligand, with the different complexes having overlapping regions of existence. For some metal ions (Hg^{2+}, Tl^{3+}, Zn^{2+}) it has been possible to derive from diffraction curves the coordination changes occurring during all the stages of the stepwise building up of halide complexes, i.e. from the solvated metal ion to the highest complex in which all solvent molecules are replaced by halide ligands. For such an analysis of the diffraction curves the concentrations of the different complexes in each solution must be known. Since concentrated solutions are needed for the diffraction measurements, stability constants, which are usually determined for dilute solutions, have to be used with care.

The structure of complexes formed between zinc and iodide in aqueous solution have been derived by a combi-

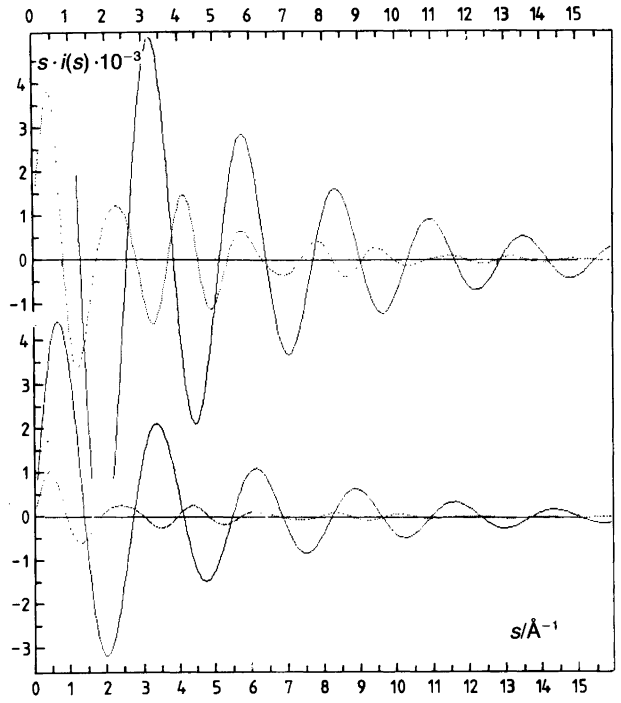

Fig. 8. Theoretical $s \cdot i(s)$ values calculated for Au-X (solid lines) and X-X (dotted lines) intramolecular interactions for a $HAuBr_4$ (upper part) and a $HAuCl_4$ (lower part) solution.

nation of X-ray diffraction and Raman spectroscopic measurements.[17] Fig. 10 shows the reduced RDF's for a series of solutions, all about 8 M in iodide concentration but with different concentrations of Zn^{2+}, with a Zn^{2+}/J^- ratio ranging from zero in a pure lithium iodide solution (Fig. 10a) to 0.5 in a pure ZnI_2 solution (Fig. 10d). Still higher values are obtained by replacing I^- by ClO_4^- (Figs. 10e and f). The complex formation results in sharp peaks in the RDF's

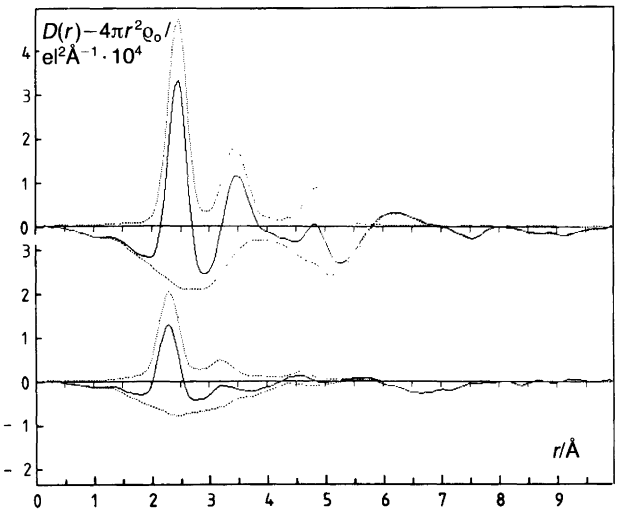

Fig. 9. Reduced radial distribution functions (solid lines) for a 3 M $HAuBr_4$ (upper curve) and a 3 M $HAuCl_4$ solution (lower curve) compared with theoretical peaks calculated for intramolecular AuX_4^- interactions. Differences between observed and calculated values are also given.

corresponding to zinc–iodide bonding distances at 2.60 Å and intramolecular iodide–iodide contact distances at 4.30 Å, which are consistent with a tetrahedral I-Zn-I angle. These interactions dominate the RDF's for the zinc iodide solutions, but minor peaks are also indicated. Iodide–water contact distances at 3.6 Å, which give the only distinct peak in pure lithium iodide (Fig. 10a), are present in all iodide-containing solutions. Zinc–water bonding distances at 2.1 Å are indicated in Figs. 10c–f, and water–water distances give a separate peak at 2.9 Å. The perchlorate-containing solutions also show peaks corresponding to the intramolecular distances in the perchlorate ion at 1.45 å (Cl-O) and 2.4 Å (O-O).

The symmetric stretching vibrations of the Zn-I bonds appear at separate frequencies in the Raman spectra (Fig. 10): for ZnI_4^{2-} at 121.6 cm^{-1}, for ZnI_3^- at 138.3 cm^{-1} and for ZnI_2 at 164.4 cm^{-1}. At low Zn/I ratios (Fig. 10b) only ZnI_4^{2-} complexes are formed, as shown by the single peak in the Raman spectrum in Fig. 10b, and an analysis of the corresponding diffraction curve or RDF gives the structural parameters for the tetrahedral ZnI_4^{2-} complex. In the remaining solutions a mixture of complexes is present. An analysis of the peaks in the Raman spectra gives the relative concentrations of the complexes, and their structures can then be derived from the diffraction curves. In the zinc perchlorate solution, with no iodide present, the zinc–water interactions at 2.1 Å are consistent with a coordination number of six. In the zinc iodide solutions corresponding zinc–water peaks are present, probably containing contributions from Zn-H_2O distances in hydrated Zn^{2+} as well as in the intermediate complexes ZnI_3^- and ZnI_2. Intramolecular I-H_2O distances in the complexes would be expected to be about the same as I-H_2O intermolecular contact distances. The presence of water molecules in the complexes cannot therefore be determined with any certainty from the diffraction curves, since the intramolecular Zn-H_2O and I-H_2O interactions cannot be separated.

The I-Zn-I angles in all the different complexes is close to tetrahedral, which makes it likely that water molecules occupy the empty tetrahedral sites in ZnI_3^- and ZnI_2. A slight decrease in the Zn-I bond lengths and a slight increase in the I-Zn-I angle is observed for the lower complexes. According to the diffraction data the maximum number of Zn-I interactions per Zn is four and the number of Zn-I interactions per J does not exceed one, which shows that I^- does not form bridges between the Zn atoms. Polynuclear complexes are not formed even in these concentrated solutions.

Several coordination changes can occur during the stepwise formation of the complexes. For thallium(III), the structures of the halide complexes formed in aqueous solution have been derived by combining diffraction measurements with NMR measurements of the Tl-205 chemical shifts.[15] The hydrated Tl^{3+} ion is octahedral. $TlBr_3$ is planar triangular, $TlBr_4^-$ is tetrahedral and the $TlCl_6^{3-}$ complex is octahedral (Table 1). Hg^{2+} changes from an octahedral arrangement in the hydrated ion, to an approximately

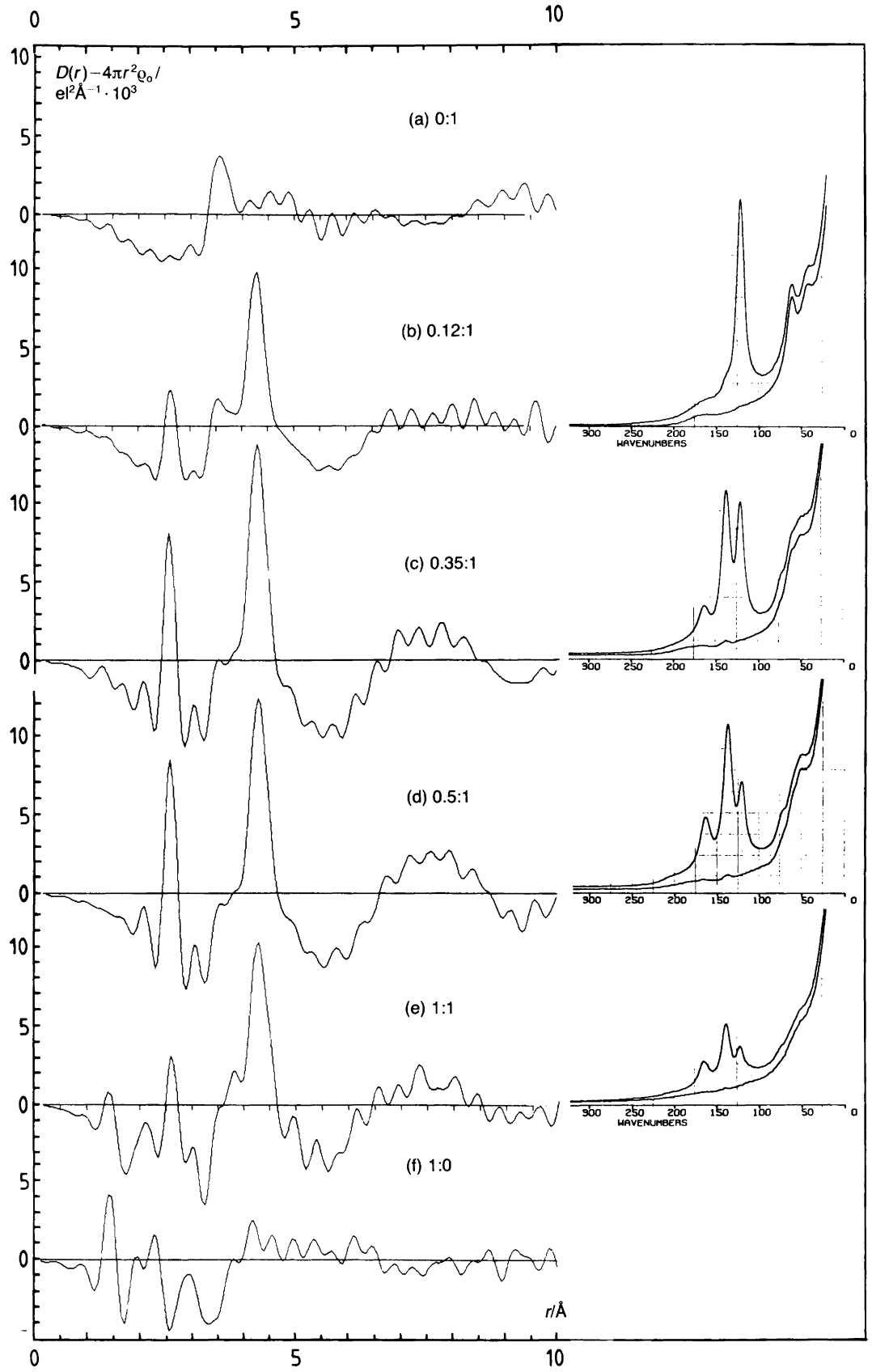

Fig. 10. Reduced radial distribution functions for a series of solutions (Li^+,Zn^{2+})(I^-,ClO_4^-) with different Zn^{2+}/I^- concentration ratios (given in the figure), from a pure lithium iodide solution (a) to a pure zinc perchlorate solution (f). The total iodide concentration is about 8 M in (a) to (d), and the total iodide and perchlorate concentration is 5 M in (e) and (f). Intensity data are normalized to a unit volume containing one I^- [(a)−(e)] or one Zn^{2+} (f). For each of the solutions (b) to (e) the Zn-I stretching region of the Raman spectrum is shown.

linear HgX_2, a flattened pyramid in HgX_3^- and a tetrahedron for HgX_4^{2-} (Table 1).[12–14]

Non-aqueous solutions are often better suited to diffraction analysis than aqueous solutions. In DMSO, solvated metal ions result in M-O as well as M-S and M-C interactions. These can be identified in the RDF's, and can be used for determining not only the solvation number but also the orientation of the bonded solvent molecule, which is not possible for a hydrated ion because of the low scattering power of hydrogen for X-rays. This also makes it possible to identify remaining solvent molecules in intermediate halide complexes of a metal ion. Diffraction measurements on DMSO solutions of mercury(II) and cadmium(II) perchlorate have shown the metal ions to form octahedral hexasolvates, with DMSO bonded through oxygen with the bond angles Hg-O-S 120.2(10)° and Cd-O-S 125.7(10)°.[18]

Only few complexes with polyatomic ligands have been investigated in solution by diffraction methods. For some common inorganic ligands, viz. NO_3^-, SO_4^{2-}, PO_4^{3-}, difficulties are encountered in identifying the metal-ligand interactions since the central ions of the ligands are light atoms and the corresponding distances fall in regions with dominant intermolecular contributions.

In sulfate complexes of Cd^{2+} [19,20] and Er^{3+} [21] in aqueous solution, the sulfate group has been found to be bonded to the metal ion as a monodentate ligand with an orientation corresponding to an M-O-S angle of about 130°, which is a magnitude also found for sulfate complexes in crystal structures.

Nitrate complexes of Ag^+ have been investigated in concentrated aqueous silver nitrate solutions[22] as well as in molten silver nitrate.[23] The same bonding of the nitrate group occurs in both media, with NO_3^- acting as a monodentate ligand with an Ag-N distance of about 3.1 Å.

Other ligands such as SCN^- are more favourable, and the structures of some thiocyanate complexes have been investigated in aqueous[24] and in DMSO[25] solutions. The results give information on the bonding of the ambidentate SCN^- ligand and its orientation relative to the metal ion.

The occurrence of complex formation in these and similar systems can be established only by uniquely identifying metal-ligand interactions in the distribution curves. When these are comparatively weak and lead to peaks in regions of the RDF's where they are overlapped by other types of interactions, a unique identification requires diffraction measurements on a series of solutions in which the concentrations of specific species are systematically varied.

Polynuclear complexes

Cluster compounds and polynuclear complexes constitute a group of complexes well suited for structure determinations in solution, in particular those complexes containing heavy atoms. The intramolecular metal–metal interactions give dominant contributions to the scattering data, and can be accurately analyzed in terms of distance, frequency and rms variation. With the compositions of the complexes and their stability constants known from other measurements and with the use of information on related crystal structures, the structures can often be derived.

As shown by Sillén and coworkers on the basis of extensive analyses of equilibrium data obtained by emf methods, the hydrolysis reactions of metal ions often lead to the formation of polynuclear complexes in which the metal ions are linked by hydroxo or oxo bridges. The removal of protons from a hydrated metal ion leads to reactions which can be written.

$$q\ M^{z+} + p\ H_2O \rightarrow M_q(OH)_p^{(qz-p)+} + p\ H^+$$

where H_2O molecules, which cannot be determined by this method, have been left out of the formulae for the metal ion complexes.

The effect on the distribution curve of the removal of protons from a slightly acidic thorium perchlorate solution is illustrated in Fig. 11.[26] It leads to the appearance of a sharp peak at 3.94 Å in the RDF, which increases with increasing hydrolysis. In crystal structures of basic thorium salts the same distance is found when two Th^{4+} ions are linked by a double hydroxo bridge, which leads to the conclusion that the same type of bridging occurs in the polynuclear hydrolysis complexes formed in solution. The average number of Th atoms bonded to each Th can be determined from the diffraction data. The absence of indications of longer Th-Th distances, as well as results from

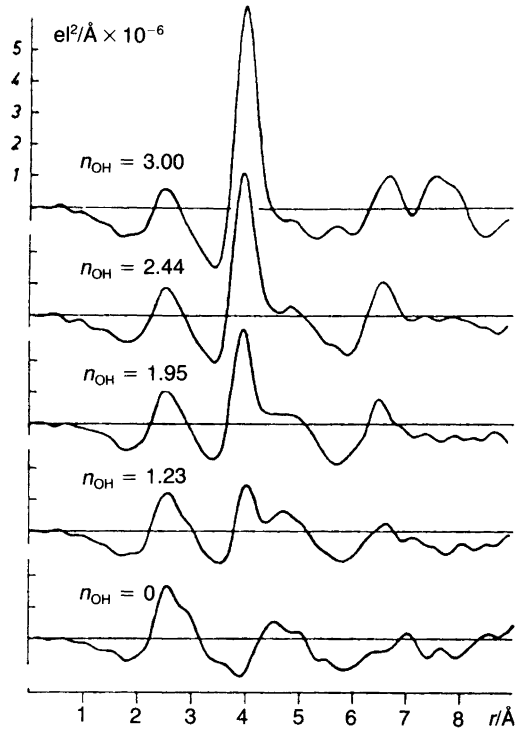

Fig. 11. Reduced distribution functions for a series of 2 M thorium perchlorate solutions of different degrees of hydrolysis, as indicated by the value of n_{OH}, which gives the average number of protons removed from each hydrated Th^{4+} ion.

equilibrium measurements, indicate the formation of dinuclear complexes, which have also been found in discrete form in crystal structures, and of complexes with a tetrahedral arrangement of the Th atoms. On further hydrolysis other Th atoms are joined to these tetrahedral groups leading to larger complexes with longer Th-Th distances.[27] The 1st coordination sphere around Th^{4+}, represented by the peak at 2.5 Å in the RDF, is largely unaffected by the hydrolysis process.

For lead(II) perchlorate solutions, emf measurements of the free hydrogen ion and the free metal ion concentrations as functions of the analytical hydrogen ion excess have established the occurrence of two dominant complexes, *viz.* $Pb_4(OH)_4^{4+}$ and $Pb_6(OH)_8^{4+}$. The radial distribution functions for two solutions, in each of which only one of the complexes is dominant, are compared in Fig. 12 with that of a weakly acidic lead perchlorate solution.[29] For the hydrolyzed solutions the distribution functions are dominated by the Pb-Pb distances within the complexes (Fig. 12). For the $Pb_4(OH)_4^{4+}$ solution only a single Pb-Pb distance is indicated, and an analysis of the peak shows three nearest Pb neighbors around each Pb. This is possible only for a tetrahedral arrangement of the Pb atoms within the complex. The contribution of the bridging OH groups to the scattering are too small for these groups to be located, but information from crystal structures makes it likely that they are positioned above the center of each tetrahedral face.

For the $Pb_6(OH)_8^{4+}$ solution, additional Pb-Pb distances are present (Fig. 12). They exclude the possibility of an octahedral arrangement of the Pb atoms in the complex, which had been suggested previously on the basis of Raman spectra, but are not sufficient for a unique derivation of the structure. The complex can, however, be isolated in crystalline form, where it appears as $Pb_6O(OH)_6^{4+}$, which consists of three face-sharing tetrahedra. Theoretical peaks, based on this structure, closely reproduce the peaks in the RDF and provide strong evidence that the structures of the complexes are the same in solution and in crystals (Fig. 12).

Although the oxygen positions in these complexes cannot usually be derived from the scattering data, their contributions to the scattering curves are in some cases sufficient for determination of their positions. In an analysis of the diffraction data for a hydrolyzed bismuth(III) perchlorate solution the presence of two different types of bridging oxygens could be established in the hydrolysis complex, which contains six octahedrally arranged Bi atoms with Bi-Bi distances of 3.69_7 Å. The bridging oxygens are situated above the tetrahedral faces of the Bi_6 complex, one group of four oxygens having Bi-O distances of 2.19 Å and the other group 2.37 Å. The formula of the complex can be written as $Bi_6O_4(OH)_4^{6+}$.[30]

Solution diffraction measurements on several other hydrolyzed metal salt solutions have lead to similar results.[31-34]

More complex structures cannot be derived on the basis of solution diffraction data alone. For known structures the contributions to a scattering curve can be calculated according to the Debye formula, and the resulting peaks in a

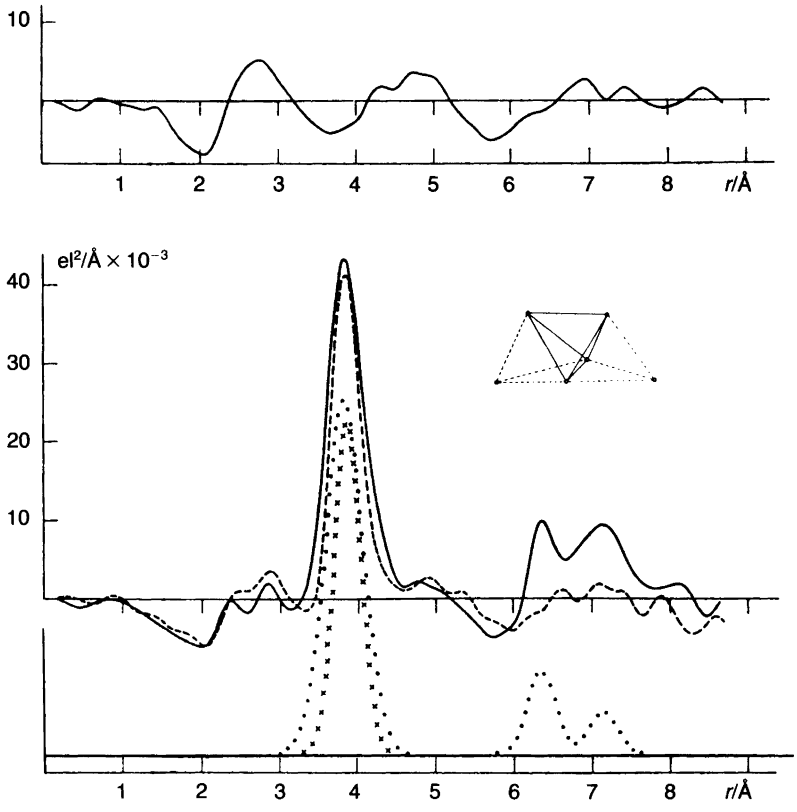

Fig. 12. Reduced distribution functions (solid lines) for 1.8 M lead(II) perchlorate solutions. The upper curve is for a slightly acidic solution ($n_{OH} = 0$) and the two lower curves for hydrolyzed solutions ($n_{OH} = 0.97$ and 1.33), where n_{OH} is the average number of protons removed from each Pb^{2+} ion. To the right is shown the arrangement of lead atoms in the tetranuclear (solid lines) and the hexanuclear (solid and dashed lines) complexes formed. Theoretical Pb-Pb peaks calculated for these structures (dotted lines) are given for comparison with the observed RDF's.

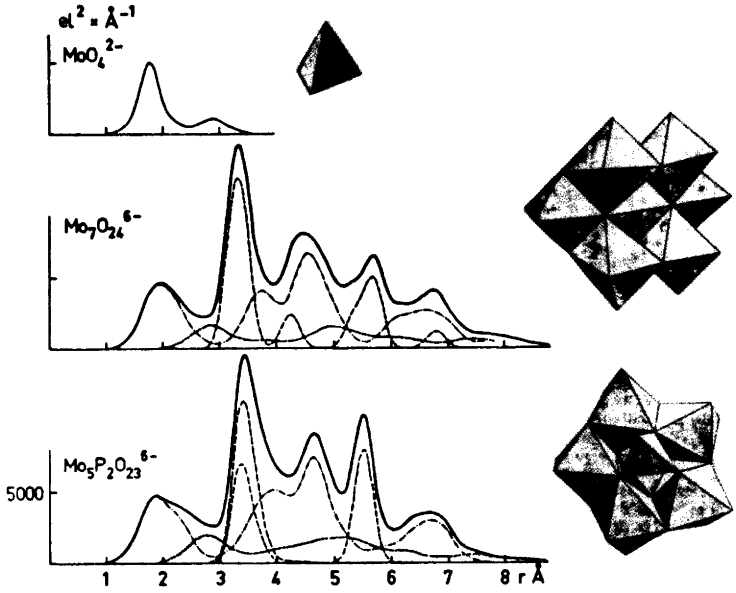

Fig. 13. Calculated shape functions for some molybdate ions. Contributions from Mo-Mo (dashed lines), Mo-O (dashed-dotted lines) and O-O (dotted lines) are shown separately.

radial distribution function can be derived by means of a Fourier transformation. The resulting function has a shape characteristic for that particular complex and can be used for identification of a complex in a solution by comparing it with the observed RDF. Structural similarities or differences can be established and changes in the structure resulting from changes in the composition of the solution can be followed.

The Fourier transforms of the calculated intensity contributions from three different molybdates are compared in Fig. 12, including the simple tetrahedral MoO_4^{2-} ion, existing in alkaline solutions, the isopolymolybdate $Mo_7O_{24}^{6-}$ and the heteropolymolybdate $Mo_5P_2O_{23}^{6-}$.[35] The calculations are based on parameter values obtained in structure determinations of crystals in which the complexes occur as discrete units. Each of the polymolybdates has a shape in which the characteristic features are primarily determined by the Mo-Mo interactions. The much larger number of O-O interactions result only in a diffuse background curve with no distinct features, while the Mo-O interactions have more distinct contributions. Despite the ordered structure of the complexes it is primarily the metal–metal interactions that can be recognized in the shape function and consequently those that can be distinguished in the distribution function for a solution containing the complex. This method has been used to identify several iso- and heteropolymolybdate ions in solution, and to follow structural changes in the complexes caused by changes in the compositions of the solutions.[36]

Conclusions

For complex chemical systems, solution diffraction data are not sufficient for the derivation of a complete model for the structure. Structural information on molecular species in the solution can, however, be derived as a result of the specific characteristics of intramolecular interactions. In some cases a separation of interactions can be made by using isomorphic substitution, which allows more detailed information to be extracted from the diffraction curves.

The structure of a heavy atom complex occurring as the dominant species in a concentrated solution can usually be uniquely and accurately determined on the basis of solution diffraction data alone. When mixtures of complexes are present and light atoms are involved, the structure derivation is less unambiguous. By comparing diffraction curves for a series of solutions in which the concentrations of specific species are systematically varied, interactions of importance for the structure determination can often be singled out and studied.

In order to obtain significant diffraction effects from a dissolved complex, relatively concentrated solutions are needed, i.e. roughly $\gtrsim 0.5$ M for the main atomic species in the complex, depending on its atomic number. In less concentrated solutions complexes are separated by layers of solvent molecules and simpler models for the intermolecular interactions can be used, which facilitates a structure derivation for the dissolved complexes. In very concentrated solutions the ordering will become more pronounced, and intermolecular interactions will lead to prominent features in the radial distribution functions. This is illustrated to some extent in Fig. 6; in this case, Cl^- ions in the concentrated solution, begin to appear in the 2nd coordination sphere of the metal ion. At still higher concentration, orientation effects similar to those in a crystal structure can be expected. A starting model for the solution can then be derived on the basis of a known crystal structure. A molten hydrate can be considered as a link between the crystal structure of the hydrate and the very concentrated solution. Comparing results from diffraction measurements on a molten hydrate with a model based on its crystal structure will give information on the restraints on

the structure that are removed in the melting process. The change in the diffraction curve when the solution is diluted can then be used in interpreting scattering data for very concentrated electrolyte solutions, the structures of which are not yet well known.

Acknowledgements. Support from the Swedish Natural Science Research Council (NFR) and from the foundation *Knut och Alice Wallenbergs Stiftelse* is gratefully acknowledged. I am indebted to E. Hansen and I. Desselberger for technical assistance.

References

1. Johansson, G. and Sandström, M. *Chem. Scr. 4* (1973) 195; Johansson, G. *Solution Diffraction Data-Handling Programs* (written in basic for an IBMPC or AT) Royal Institute of Technology, Stockholm 1985.
2. Bol, W., Gerritis, G. J. H. and van Eck, C. L. vP. *J. Appl. Crystallogr. 3* (1970) 486.
3. Soper, A. K., Neilson, G. W., Enderby, J. E. and Howe, R. A. *J. Phys. C 10* (1977) 1793.
4. Enderby, J. E. and Neilson, G. W. In: Franks, F., Ed., *Water a Comprehensive Treatise,* Plenum Press, New York 1981.
5. Enderby, J. E. *Pure Appl. Chem. 57* (1985) 1025.
6. Narten, A. H., Vaslow, F. and Levy, H. A. *J. Chem. Phys. 58* (1973) 5017.
7. Pálinkás, G. and Kálmán, E. In: Hargittai, I. and Orville-Thomas, W. J., Eds., *Diffraction Studies on Non-Crystalline Substances,* Elsevier, Amsterdam 1981.
8. Caminiti, R., Licheri, G., Piccaluga, G., Pinna, G. and Magini, M. *Rev. Inorg. Chem. 1* (1979) 333.
9. Ohtaki, H. *Rev. Inorg. Chem. 4* (1982) 103.
10. Maeda, M., Ohtaki, H. and Johansson, G. *Bull. Chem. Soc. Jpn. 47* (1974) 2229.
11. Maeda, M., Akaishi, T. and Ohtaki, H. *Bull. Chem. Soc. Jpn. 48* (1975) 3193.
12. Gaizer, F. and Johansson, G. *Acta Chem. Scand. 22* (1968) 3013.
13. Sandström, M. and Johansson, G. *Acta Chem. Scand., Ser. A 31* (1977) 132.
14. Sandström, M. *Acta Chem. Scand., Ser. A 32* (1978) 627.
15. Glaser, G. and Johansson, G. *Acta Chem. Scand., Ser. A 36* (1982) 125.
16. Goggin, P. L., Johansson, G., Maeda, M. and Wakita, H. *Acta Chem. Scand., Ser. A 38* (1984) 625.
17. Carr, C., Johansson, G., Sandström, M. and Wakita, H. *To be published.*
18. Sandström, M., Persson, I. and Ahrland, S. *Acta Chem. Scand., Ser. A 32* (1978) 607.
19. Caminiti, R. and Johansson, G. *Acta Chem. Scand., Ser. A 35* (1981) 373.
20. Caminiti, R. *Z. Naturforsch., A 36* (1981) 1062.
21. Johansson, G. and Wakita, H. *Inorg. Chem. 24* (1985) 3047.
22. Yamaguchi, T., Johansson, G., Holmberg, B., Maeda, M. and Ohtaki, H. *Acta Chem. Scand., Ser. A 38* (1984) 437.
23. Holmberg, B. and Johansson, G. *Acta Chem. Scand., Ser. A 37* (1983) 367.
24. Persson, I., Iverfeldt, Å. and Ahrland, S. *Acta Chem. Scand., Ser. A 35* (1981) 295.
25. Ohtaki, H. *Pure Appl. Chem. 59* (1987) 1143.
26. Johansson, G. *Acta Chem. Scand. 22* (1968) 399.
27. Magini, M., Cabrini, A., Scibona, G., Johansson, G. and Sandström, M. *Acta Chem. Scand., Ser. A 30* (1976) 437.
28. Sillén, L. G. and Martell, A. E. *Stability Constants,* Special Publication No. 17, The Chemical Society, London 1964.
29. Johansson, G. and Olin, Å. *Acta Chem. Scand. 22* (1968) 3197.
30. Sundvall, B. *Acta Chem. Scand., Ser. A 34* (1980) 93.
31. Johansson, G. and Ohtaki, H. *Acta Chem. Scand. 27* (1973) 643.
32. Åberg, M. *Acta Chem. Scand. 24* (1970) 2901.
33. Johansson, G. *Acta Chem. Scand. 20* (1966) 553.
34. Caminiti, R., Johansson, G. and Toth, I. *Acta Chem. Scand., Ser. A 40* (1986) 435.
35. Johansson, G., Pettersson, L. and Ingri, N. *Acta Chem. Scand., Ser. A 28* (1974) 1119.
36. Johansson, G., Pettersson, L. and Ingri, N. *Acta Chem. Scand., Ser. A 32* (1978) 407; *Ibid.* 439; *Ibid.* 681; *Ibid. Ser. A 33* (1979) 305; *Ibid. Ser. A 35* (1981) 181.
37. Nilsson, R. O. *Arkiv Kemi 12* (1958) 513.
38. Gaizev, F. and Johansson, G. *Acta Chem. Scand., Ser. A 42* (1988) 209.
39. Johnsson, M. and Persson, I. *Inorg. Chim. Acta 130* (1987) 215.
40. Ohtaki, H., Maeda, M. and Ito, S. *Bull. Chem. Soc. Jpn. 49* (1974) 2217.
41. Tsurumi, M., Maeda, M. and Ohtaki, H. *Denki Kagaku 45* (1977) 367.
42. Pocev, S., Triolo, R. and Johansson, G. *Acta Chem. Scand., Ser. A 33* (1979) 179.
43. Caminiti, R., Licheri, G., Paschina, G., Piccaluga, G. and Pinna, G. *Z. Naturforsch., A 35* (1980) 1361.
44. Ichihashi, M., Wakita, H. and Masuda, I. *J. Solution Chem. 13* (1984) 505.
45. Magini, M. *J. Chem. Phys. 74* (1981) 2523.
46. Lee, H.-G., Matsumoto, Y., Yamaguchi, T. and Ohtaki, H. *Bull. Chem. Soc. Jpn. 56* (1983) 443.
47. Paschina, G., Piccaluga, G., Pinna, G. and Magini, M. *Chem. Phys. Lett. 98* (1983) 157.
48. Musinu, A., Paschina, G., Piccaluga, G. and Magini, M. *J. Chem. Phys. 80* (1984) 2772.
49. Magini, M. *J. Chem. Phys. 73* (1980) 2499.
50. Ichihashi, M., Wakita, H., Mibuchi, T. and Masuda, I. *Bull. Chem. Soc. Jpn. 55* (1982) 3160.
51. Wertz, D. L. and Tyvoll, J. L. *J. Inorg. Nucl. Chem. 36* (1974) 3713.
52. Brady, G. W. *J. Chem. Phys. 29* (1958) 1371.
53. Brady, G. W., Robin, M. B. and Varimbi, J. *Inorg. Chem. 3* (1964) 1168.
54. Magini, M. and Radnai, T. *J. Chem. Phys. 71* (1979) 4255.
55. Wertz, D. L. and Steele, M. L. *Inorg. Chem. 19* (1980) 1652.
56. Luter, M. D. and Wertz, D. L. *J. Phys. Chem. 85* (1981) 3542.
57. Magini, M. *J. Chem. Phys. 76* (1982) 1111.
58. Wertz, D. L. and Kruh, R. F. *J. Chem. Phys. 50* (1969) 4013.
59. Van Eck, C. L. vP., Wolters, H. B. M. and Jaspers, W. J. M. *Recl. Trav. Chim. Pays-Bas 75* (1956) 802.
60. Sandström, M. *Acta Chem. Scand., Ser. A 31* (1977) 141.
61. Ahrland, S., Hansson, E., Iverfeldt, Å. and Persson, I. *Acta Chem. Scand., Ser. A 35* (1981) 275.
62. Persson, I., Sandström, M., Goggin, P. L. and Mosset, A. *J. Chem. Soc., Dalton Trans.* (1985) 1597.
63. Iverfeldt, Å. and Persson, I. *Inorg. Chim. Acta 111* (1986) 171.
64. Sandström, M., Persson, I. and Goggin, P. L. *J. Chem. Soc., Dalton Trans.* (1987) 2411.
65. Steele, M. L. and Wertz, D. L. *J. Am. Chem. Soc. 98* (1976) 4424.
66. Smith, L. S., McCain, D. C. and Wertz, D. L. *J. Am. Chem. Soc. 98* (1976) 5125.
67. Wertz, D. L. and Finch, S. T. *Inorg. Chem. 18* (1979) 1590.
68. Caminiti, R. and Cucca, P. *Chem. Phys. Lett. 89* (1982) 110.
69. Magini, M., deMoraes, M., Licheri, G. and Piccaluga, G. *J. Chem. Phys. 83* (1985) 5797.
70. Wakita, H., Ichihashi, M., Mibuchi, T. and Masuda, I. *Bull. Chem. Soc. Jpn. 55* (1982) 817.

71. Magini, M., Paschina, G. and Piccaluga, G. *J. Chem. Phys. 76* (1982) 1116.
72. Caminiti, R., Atzci, D., Cucca, P., Squintu, F. and Bongiovanni, G. *Z. Naturforsch., A 40* (1985) 1319.
73. Glaser, J., Goggin, P. L., Sandström, M. and Lutsko, V. *Acta Chem. Scand., Ser. A 36* (1982) 55.
74. Glaser, J. *Acta Chem. Scand., Ser. A 36* (1982) 451.
75. Wertz, D. L., Lawrence, R. M. and Kruh, R. F. *J. Chem. Phys. 43* (1965) 2163.
76. Kalman, E., Serke, I., Palinkas, G., Johansson, G., Kabisch, G., Maeda, M. and Ohtaki, H. *Z. Naturforsch., A 38* (1983) 225.
77. Steele, M. L. and Wertz, D. L. *Inorg. Chem. 16* (1977) 1225.
78. Kruh, R. F. and Standley, C. L. *Inorg. Chem. 1* (1962) 941.
79. Wertz, D. L. and Bell, J. R. *J. Inorg. Nucl. Chem. 35* (1973) 137.
80. Wertz, D. L. and Bell, J. R. *J. Inorg. Nucl. Chem. 35* (1973) 861.
81. Yamaguchi, T. and Ohtaki, H. *Bull. Chem. Soc. Jpn. 51* (1978) 3227.
82. Dagnall, S. P., Hague, D. N. and Towl, A. D. C. *J. Chem. Soc., Faraday Trans. 2, 79* (1983) 1817.
83. Paschina, G., Piccaluga, G., Pinna, G. and Magini, M. *J. Chem. Phys. 78* (1983) 5745.
84. Tajiri, Y., Ichihashi, M., Mibuchi, T. and Wakita, H. *Bull. Chem. Soc. Jpn. 59* (1986) 1155.

Received May 27, 1988.